Scientific Research Publishing

Open Journal of Geology, 2025, 15(7), 377-389
https://www.scirp.org/journal/ojg
ISSN Online: 2161-7589
ISSN Print: 2161-7570

Characteristics of Fluorescent Organic Matter Entrapped in Silica Sinter from the Western Shore of Lake Shikaribetsu, Hokkaido, Japan

Shigenori Ogihara

Faithful Crystals, Tokyo, Japan
Email: faithful.love.crystals@gmail.com

How to cite this paper: Ogihara, S. (2025) Characteristics of Fluorescent Organic Matter Entrapped in Silica Sinter from the Western Shore of Lake Shikaribetsu, Hokkaido, Japan. *Open Journal of Geology*, **15**, 377-389.
https://doi.org/10.4236/ojg.2025.157019

Received: April 23, 2025
Accepted: July 26, 2025
Published: July 29, 2025

Abstract

Small streams flowing into the western shore of Lake Shikaribetsu in Hokkaido are surrounded by extensive volcanic ejecta from the Shikaribetsu volcanic group, where layered silica sinters are exposed. These sinters exhibit strong fluorescence. In this study, the fluorescent silica sinters were classified into three types based on their fluorescence colors: orange, purple, and yellow. The objective of this research was to identify the organic compounds responsible for the fluorescence observed in each category. Particular focus was placed on analyzing hydrocarbon and polycyclic aromatic hydrocarbon (PAH) fractions. The PAHs in the orange fluorescent sinters were dominated by alkylated PAHs, suggesting a petrogenic origin. In contrast, PAHs in the yellow fluorescent sinters consisted mainly of unsubstituted (naked) PAHs, including 7-ring PAHs, indicating a possible pyrogenic (combustion-derived) origin. However, the maximum thermal history of the organic matter, estimated from maturity indices, does not exceed 150˚C—a temperature insufficient to account for the high-temperature conditions typically required for the formation of pyrogenic PAHs. Additionally, the fluorescence colors of the sinters do not correspond to the fluorescence characteristics of the identified PAHs. It is therefore likely that the compounds responsible for the observed fluorescence are contained within other fractions not analyzed in this study, such as ketones, esters, or alcohols.

Keywords

Fluorescent Organic Matter, GC/MS, Lake Shikaribetsu, PAH, Silica Sinter

1. Introduction

On the western shore of Lake Shikaribetsu, located in central Hokkaido, northern

Japan (Figure 1), silica sinters found in streams exhibit red, yellow, and purple fluorescence. In general, fluorescence observed in minerals is typically not derived from their primary components, but rather from trace elements. Elements such as Ti, V, Cr, Mn, Cu, Ag, Sn, W, Tl, Pb, Bi, U, Sc, Y, and rare earth elements (REEs) are well-documented contributors to mineral fluorescence (e.g., [1]). For example, the yellow fluorescence of the opal variety known as hyalite has been attributed to trace amounts of uranium [2].

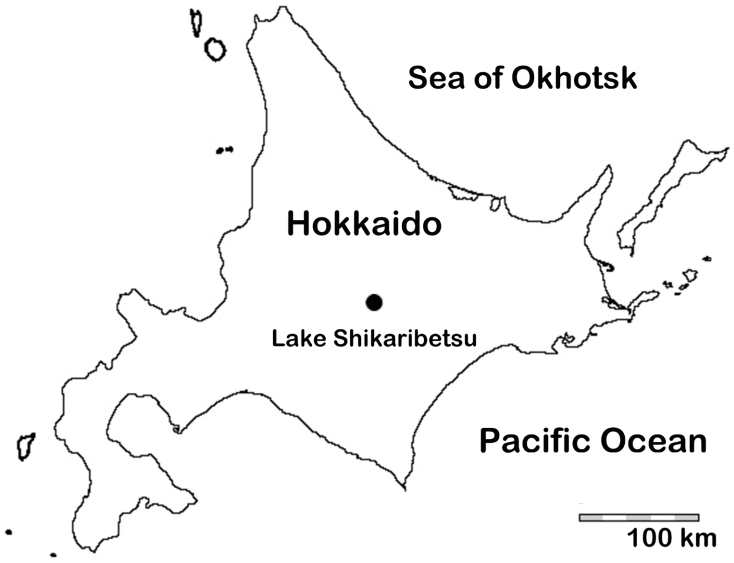

Figure 1. Map showing the location of study area.

Early studies hypothesized that the fluorescence observed in Shikaribetsu opal was similarly caused by inorganic trace elements. However, subsequent investigations by [3] and [4], which conducted detailed inorganic analyses to determine the origin of the fluorescence in Shikaribetsu opal, failed to identify any definitive inorganic source. Their results instead suggested the possibility that the fluorescence might originate from organic substances.

2. Occurrence of Silica Sinter

Lake Shikaribetsu is located in central Hokkaido, approximately 100 km west of Sapporo. It is a dammed lake formed by volcanic activity that occurred between 10,000 and 60,000 years ago, which blocked the flow of the Shikaribetsu River. The lake has a circumference of approximately 13 km. On the western slope of the lake, volcanic ejecta composed of pyroxene andesite are distributed, with several streams flowing into the lake. The fluorescent silica sinters in this area are valley-filling deposits that have formed by the infilling of these streams.

Silica sinter deposits are found at two distinct locations along the stream: an upstream section (upper layer) with a thickness of approximately 2 - 4 meters, and a downstream section (lower layer) with a thickness of approximately 4 - 6 meters. This area is located within a designated national park.

Near the silica sinter outcrops on the western slope of Lake Shikaribetsu, the remains of an abandoned mine can be observed. However, no historical mining records exist, and the purpose of the mining activities remains unclear. There are documented records of mercury mining at the Uramaku Mercury Mine, located 8 km northwest of Lake Shikaribetsu, and the Tokachi Mercury Mine, 8 km to the east. Several hot springs are also found in the surrounding area, including the lakeside hot spring on the shore of Lake Shikaribetsu, Yamada Hot Spring near the northern inlet, and Sugano Hot Spring beyond the mountain to the west of the lake—all characterized by neutral pH waters.

The samples used in this study were obtained from the former Geological Department Collection of the University of Tokyo. The author did not participate in the survey, which was conducted several decades ago, and many details of the survey records are unclear.

3. Sample Description

For various analyses, fist-sized samples were collected. These samples were cut perpendicular to their layered structures, polished, and examined under both normal light and black light (360 nm). In addition, thin sections were prepared for further microscopic examination. Through macroscopic, fluorescent, and microscopic observations, the following sequence of sinter layers was identified. The colours described in this study were determined by naked eye and no spectroscopic analysis was performed (Figure 2).

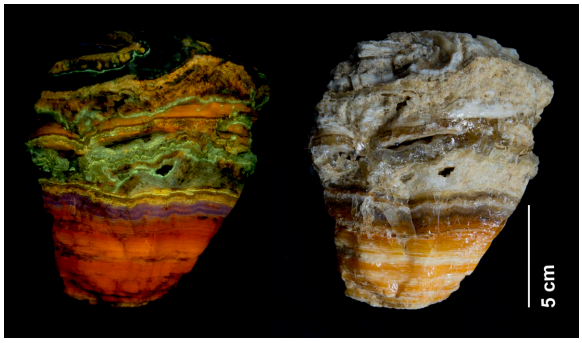

Figure 2. Photographs of silica sinter sample under normal light (right) and ultraviolet rays (365 nm) (left).

Orange to Brown Sinter Layer (up to approximately 10 cm thick): This layer exhibits thin laminae (Figure 3(A)) and emits a strong orange fluorescence under black light.

Transparent, Massive Sinter Layer (3 - 5 cm thick): Overlying the orange sinter, this layer is composed of high-purity silica, characterized by a glossy, conchoidal fracture surface. Under black light, it displays a purple fluorescence.

White, Partially Resinous Sinter Layer: This layer transitions abruptly from the orange sinter layer. The white portion itself is non-fluorescent, but resinous areas within it display undulating layers of yellow fluorescent spots (Figure 3(B) and

Figure 3(C)). These fluorescent spots range from 0.1 to 0.2 mm in size. Under the microscope, the resinous fluorescent material exhibits upward growth patterns and occurs in several stacked layers, coexisting with authigenic diatom fossils, which are densely packed in certain areas. The resinous fluorescent material lacks the branching or segmented structures typical of algae. The fluorescent layers are situated above horizons densely packed with plant fragments, which are incorporated into the fluorescent layers and have undergone silicification. Notably, such dense accumulations of plant fragments are not observed elsewhere in the sequence.

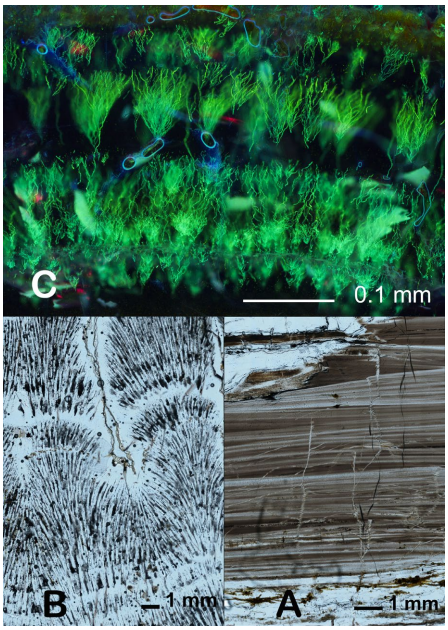

Figure 3. Photomicrographs of thin section of silica sinter (open Nicol). A: Orange fluorescent sinter, B: Yellow fluorescent sinter, C: Yellow fluorescent dots exhibiting dendritic structures under ultraviolet rays.

The orange, purple, and yellow fluorescent sinter layers were each powdered using a mortar and subsequently used for further analyses.

4. Compound Identification

Traditional Soxhlet extraction using dichloromethane/methanol (93/7, v/v) was performed for 70 h to extract the biomarker. The extracted solvent was concentrated using a rotary evaporator. The isolated lipid was divided into four fractions using silica-gel column chromatography. A hydrocarbon fraction was obtained using two column volumes of n-hexane; a polyaromatic hydrocarbon fraction was obtained with two volumes of n-hexane/dichloromethane (2/1, v/v); an aliphatic ketone/ester fraction was obtained with seven volumes of n-hexane/dichloromethane (1/1, v/v); and a polar fraction was obtained with excess dichloromethane/methanol (1/1, v/v). Then, two fractions were examined via GC/MS: one corresponding to hydrocarbons, another to polyaromatic hydrocarbons.

A Shimadzu QP-2010 plus GC-MS system equipped with a 30-m fused silica capillary column (Thermo Scientific TG-5MS 0.25 mm i.d., 0.25 μm film thickness) and a splitless column injector was used. The following temperature program was utilized: isothermal conditions at 60˚C for 1 min; 60˚C - 175˚C at 10˚C/min; 175˚C - 225˚C at 6˚C/min; 225˚C - 300˚C at 4˚C/min; and isothermal conditions at 300˚C for 20 min. MS data were recorded in the electron impact mode at 70 eV scanning from m/z 50 to m/z 520. This methodology corresponds to the typical analysis for biomarkers.

The structures of organic compounds were determined based on mass spectrometry (MS) spectra and the retention indices of naked polycyclic aromatic hydrocarbons (PAHs). Naked PAHs, ranging from naphthalene to coronene, were identified by comparing their MS spectra and retention indices with those of standard reference materials. PAHs with molecular weights greater than that of coronene were identified with reference to the studies by [5] and [6]. Alkylbenzenes were primarily identified according to the classification proposed by [7]. Other compounds were identified by comparison with the NIST05 mass spectral database.

5. Organic Geochemical Analysis Results

5.1. Orange Fluorescent Layer

5.1.1. Hydrocarbon Fraction

The total ion chromatogram (TIC) of the hydrocarbon fraction from the orange fluorescent layer is shown in **Figure 4** (top panel). This fraction contains *n*-alkanes ranging from C_{10} to C_{24}, with a predominance in the C_{15} to C_{22} range. No significant predominance of either odd- or even-carbon-numbered *n*-alkanes was observed. Cyclic biomarkers, such as steranes and hopanes, were detected in trace amounts. A notable feature of this fraction is the presence of sulfur. Dodecylbenzene was detected, eluting just before *n*-C_{19}. Among the alkylbenzenes, only this dodecyl-substituted compound was identified.

5.1.2. PAH Fraction

The PAH fraction is illustrated in **Figure 4** (bottom panel). Major components include naphthalene (A), acenaphthylene (B), phenanthrene (C), 4H-cyclopenta-[def]phenanthrene (D), pyrene (E), and chrysene (F), along with their methyl-(C1), ethyl-(C2), and dimethyl-(C2) derivatives, which dominate this fraction. The relatively high abundance of these alkylated derivatives is a distinctive feature of this sample. Trace amounts of perylene (I) were also detected, representing the highest-carbon-number PAH identified in this sample.

Using the phenanthrene concentration in the maturity formula Ro = 0.38 + 0.61 × MPI-1 [8], the calculated vitrinite reflectance (Ro) value is 0.82.

Additionally, C1- and C2-substituted naphthalenes were observed in the extended hydrocarbon fraction (middle panel), eluting prior to the PAH fraction. No thiophenes, other sulfur-containing PAHs, or phenyl-substituted PAHs were detected in this layer.

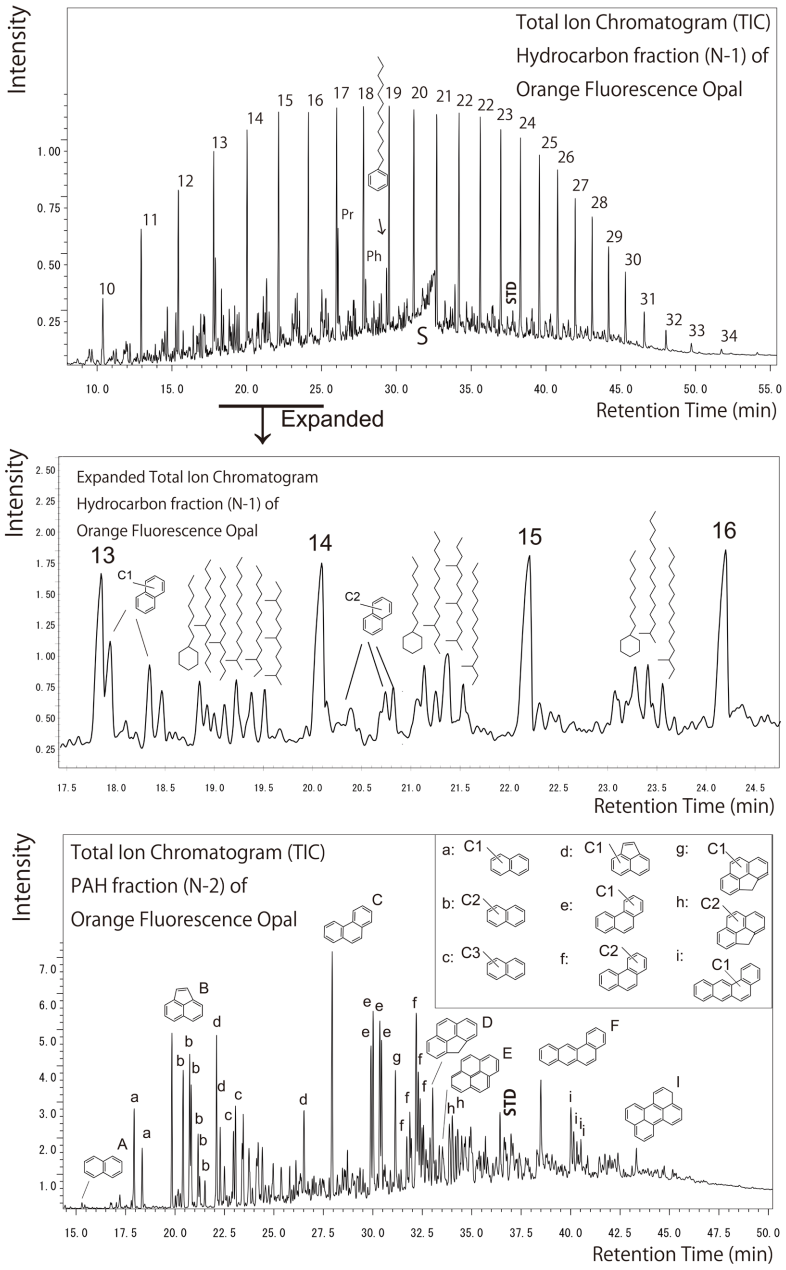

Figure 4. Total ion chromatogram of hydrocarbon fraction (upper) and expanded chromatogram (middle) and PAH fraction (bottom) extracted from orange fluorescence silica sinter. Arabic numbers are showing the number of carbon of *n*-alkane. The names of the compounds indicated by the alphabets at the bottom figure are shown in the table.

5.2. Purple Fluorescent Layer

5.2.1. Hydrocarbon Fraction

The total ion chromatograms (TICs) for the hydrocarbon and PAH fractions of the purple fluorescent layer are shown in **Figure 5**. The hydrocarbon fraction contains n-alkanes ranging from C_{18} to C_{22}, with a predominance at C_{22} and C_{23}. For *n*-alkanes above C_{27}, an odd-over-even carbon number preference was observed. Cyclic biomarkers such as hopanes and steranes were not detected in this layer.

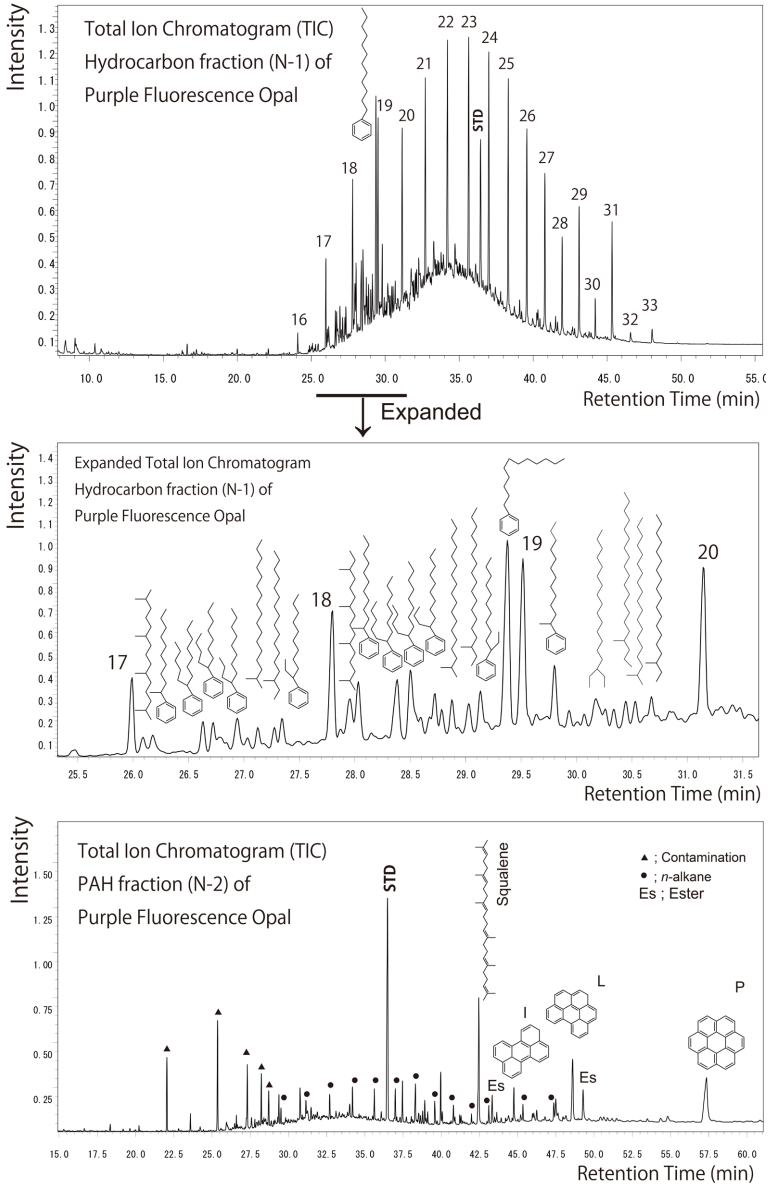

Figure 5. Total ion chromatogram of hydrocarbon fraction (upper) and expanded chromatogram (middle) and PAH fraction (bottom) extracted from purple fluorescence silica sinter. Arabic numbers are showing the number of carbon of *n*-alkane. The names of the compounds indicated by the alphabets at the bottom figure are shown in the table.

A distinct unresolved complex mixture (UCM) peak was observed near C_{22}. The pristane/phytane (Pr/Ph) ratio was 0.85, and the phytane/n-C_{18} (Ph/C_{18}) ratio was 0.19. In contrast to the orange fluorescent layer, no sulfur-containing compounds were detected in this layer. Dodecylbenzene was again detected, eluting just before n-C_{19}. Thiophenes, other sulfur-containing PAHs, and phenyl-substituted PAHs were also absent.

The expanded view in the middle panel of **Figure 5** shows the elution of iso- and anteiso-alkanes between the n-alkane peaks. Additionally, various branched alkylbenzenes were identified.

5.2.2. PAH Fraction

The total ion chromatogram (TIC) of the PAH fraction is shown in the bottom panel of Figure 5. Detected PAHs include perylene (I), benzo[ghi]perylene (L), and coronene (P), with coronene being relatively abundant. No alkyl-substituted PAHs were detected in this fraction. The methyl phenanthrene index (MPI-1) was calculated to be 0.64.

Squalene was identified as the largest peak in the chromatogram. Additionally, contaminants from the vinyl sample storage bag (▲) were detected, as well as *n*-alkanes (●) that had carried over from the hydrocarbon fraction. Esters, originating from the ketone-ester fraction, were also found to have eluted into the PAH fraction.

5.3. Yellow Fluorescent Sinter

5.3.1. Hydrocarbon Fraction

The total ion chromatograms (TICs) for the hydrocarbon and PAH fractions extracted from the yellow fluorescent sinter are shown in Figure 6 (top panel). *n*-Alkanes ranging from C_{14} to C_{24} were detected, with a predominance at C_{22} to C_{24}. For *n*-alkanes above C_{27}, an odd-over-even carbon number preference was observed. The carbon preference index (CPI, C_{20} - C_{34}) was calculated to be 1.10. No cyclic biomarkers, such as hopanes or steranes, were detected.

Dodecylbenzene eluted just before *n*-C_{19}, and no sulfur-containing compounds were identified. A bimodal unresolved complex mixture (UCM) was observed, with peaks centered near C_{19} and C_{22}.

The pristane/phytane (Pr/Ph) ratio was 0.63, and the phytane/*n*-C_{18} (Ph/C_{18}) ratio was 0.57. Thiophenes and other sulfur-containing PAHs were absent. However, the phenyl-PAH compound 1,2'-Binaphthyl was detected. In the middle panel of Figure 6, compounds eluting between *n*-C_{17} and *n*-C_{20} are shown. Detected compounds include pristane, phytane, iso- and anteiso-alkanes, as well as various branched alkylbenzenes. This chromatogram closely resembles the expanded hydrocarbon fraction observed in the purple fluorescent sinter.

5.3.2. PAH Fraction

The PAH fraction is presented in the bottom panel of Figure 6. A broad spectrum of PAHs was identified, ranging from the 3-ring phenanthrene (C) to the 7-ring coronene (P), including dibenzo [cd, lm] perylene (R) and dibenzo [a, h] pyrene (S). Among these, benzo[ghi]perylene (L) was the most abundant compound, followed by benzo[j]fluoranthene (H) and perylene (I). A notable characteristic of this sample is the presence of additional 6-ring and 7-ring PAHs beyond coronene.

In addition, a methyl-substituted derivative of benzo[ghi]perylene, methylbenzo[ghi]perylene (M), was identified. Other PAHs also exhibited methyl-substituted forms, although their concentrations were relatively low. The methyl phenanthrene index (MPI-1) was calculated to be 0.61. Using the equation Ro = 0.38 + 0.61 × MPI-1 [7], the equivalent vitrinite reflectance (Ro) was estimated to be 0.75.

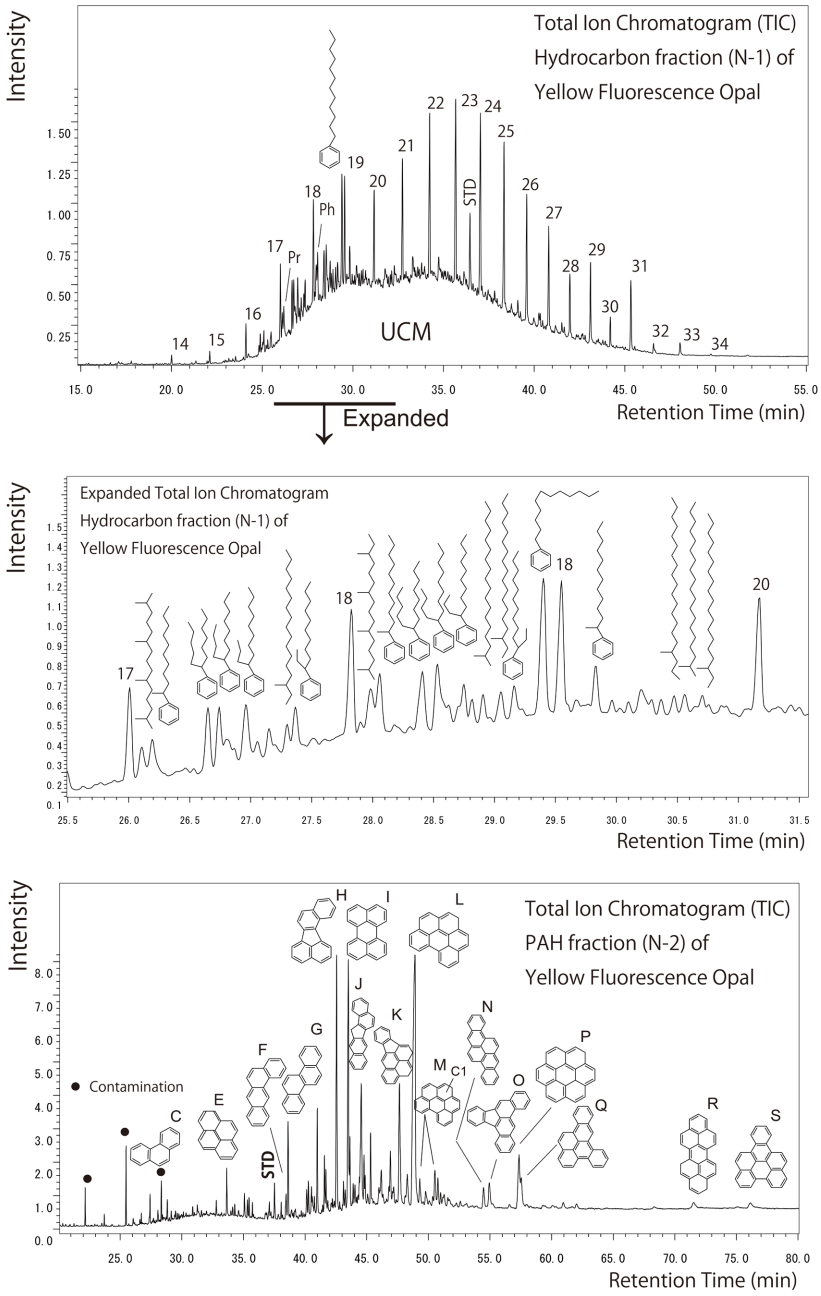

Figure 6. Total ion chromatogram of hydrocarbon fraction (upper) and expanded chromatogram (middle) and PAH fraction (bottom) extracted from yellow fluorescence silica sinter. Arabic are showing the number of carbon of *n*-alkane. The names of the compounds indicated by the alphabets at the bottom figure are shown in the table.

6. Origin of PAHs

Table 1 presents the amount of PAHs extracted from each fluorescent sinter. The purple fluorescent sinter is excluded from the discussion of origins due to the minimal quantity detected. When discussing the origin of PAHs, they are broadly classified into two categories: petrogenic (oil-derived) and pyrogenic (combustion-derived) PAHs [8].

Table 1. Peak for identified compounds in GC/MS chromatograms and each content.

Compound	Mark in figure	Color of fluorscence		
		Orange	Purple	Green
Naphthalene	A	0.8		
Acenaphthylene	B	7.5		
Phenanthrene	C	15		0.8
4H-cyclopenta[def]phenantherene	D	10		
Pyrene	E	4.7		12
Chrysene	F	3.0		15
1,2'-Binaphthyl	G			19
Benzo[j]fluoranthene	H			62
Perylene	I	2.0	2.0	64
13H-Dibendo[a, h]fluorene	J			45
Indeno[1,2,3-cd]pyrene	K			46
Benzo[ghi]perylene	L		5.6	160
Methyl-benzo[ghi]perylene	M			16, 18
Dibenzo[b, def]chrysene	N			14
Dibenzo[a, e]fluoranthene	O			12
Coronene	P		9.2	24
Benzo[a, e]picene	Q			13
Dizenzo[cd, lm]perylene	R			4.9
Dizenzo[a, h]pyrene	S			3.8
Total		43	17	480
				ng/g-sample

The petrogenic category includes organic compounds formed through diagenesis, crude oil, and its seepages. There is a significant compositional difference between petrogenic and combustion-derived PAHs: combustion-derived types are typically non-alkylated (naked) PAHs, whereas petrogenic-derived types consist predominantly of alkylated PAHs. This distinction is further discussed in sources such as [9] [10] for petrogenic PAHs and [11] for pyrogenic PAHs.

The PAHs in the orange fluorescent sinter, which contain a high proportion of alkylated PAHs, correspond to petrogenic-derived PAHs. In contrast, the PAHs in the yellow fluorescent sinter, dominated by non-alkylated (naked) PAHs, correspond to pyrogenic (combustion-derived) PAHs.

The formation temperatures of these two types differ significantly: petrogenic PAHs form at temperatures between 100˚C and 150˚C, while pyrogenic PAHs form at much higher temperatures, ranging from 350˚C to 1200˚C [12] and [13].

Specifically, the PAHs in the yellow fluorescent silica sinter include 7-ring PAHs, suggesting their formation at high temperatures. This temperature is significantly higher than typical surface organic matter temperatures, indicating an unusually high-temperature origin. A plausible high-temperature origin in this context is wildfire. The average ground temperature during forest fires is approximately 850˚C [14], which falls within the temperature range for the formation of pyrogenic PAHs. Wildfires are therefore considered one of the potential origins of these PAHs.

Previous studies have reported that organic matter and PAHs are often highly concentrated in post-wildfire soil and ash [15]-[17]. These studies have documented PAHs of wildfire origin, underscoring the significant contribution of forest fires to the generation of pyrogenic PAHs.

In recent years, a correlation between PAH accumulation mechanisms and mercury deposits has been highlighted. This suggests that mercury-rich environments may play a role in the concentration or formation of PAHs. Karpatite ($C_{24}H_{12}$: coronene) and idrialite ($C_{22}H_{14}$: picene) are well-known to occur widely in hydrothermal mercury deposits [18] and [19]. This association highlights a potential link between PAHs and mercury-rich geological environments. Additionally, karpatite from the New Idria region in California has been identified as having a sedimentary origin and was generated during the final stages of hydrothermal activity [20]. The New Idria region hosts numerous mercury deposits [21], and karpatite itself is found coexisting with cinnabar (HgS) [19].

Within a 10 km radius of Lake Shikaribetsu, historical records indicate the presence of several active mercury mines. Additionally, near the silica sinter deposits, there are multiple abandoned mines of unknown purpose. To elucidate the origin of the fluorescent compounds in the silica sinter, it is essential to investigate the potential correlation between these compounds and the mining activities in the area.

Analysis of the fluorescent ketone/ester fraction and alcohol fraction is currently underway and was not able to be shown in this study. This will be clarified through future analysis.

7. Summary

The western shore of Lake Shikaribetsu in Hokkaido is surrounded by extensive volcanic ejecta from the Shikaribetsu volcanic group, where layered silica sinters are exposed. These sinters exhibit strong fluorescence and were classified into three types based on their fluorescence colors: orange, purple, and yellow. Special attention was given to the analysis of hydrocarbon and polycyclic aromatic hydrocarbon (PAH) fractions. The PAHs in the orange fluorescent sinters were predominantly alkylated, suggesting a petrogenic origin. In contrast, the PAHs in the yellow fluorescent sinters mainly consisted of unsubstituted (naked) PAHs, including 7-ring PAHs, pointing to a possible pyrogenic (combustion-derived) origin.

Recent studies have revealed a link between PAH formation and the presence

of mercury mines. Historical records show several active mercury mines within a 10 km radius of Lake Shikaribetsu. Additionally, there are multiple abandoned mines near the silica sinter deposits with an unknown purpose. To clarify the origin of the fluorescent compounds in the silica sinters, further investigation into the potential correlation with past mining activities in the area is needed.

Acknowledgements

This study summarizes the results of student training at the Faculty of Science, University of Tokyo, over the past 18 years. We would like to express our gratitude to the students who participated in the workshop and contributed original reports. In particular, Miss Momoyo Suetomi has been extremely helpful in making presentation at the Gemmological Society of Japan.

Conflicts of Interest

The author declares no conflicts of interest regarding the publication of this paper.

References

[1] Robbins, M.A. (1983) The Collector's Book of Fluorescent Minerals. Edited by Robbins, M.A., Springer Science and Business Media, LLC., 184.

[2] Graetsch, H. (1994) Structural Characteristics of Opaline and Microcrystalline Silica Minerals. *Reviews in Mineralogy*, **29**, 209-232.

[3] Okazaki, C., Matsueda, H., Kanai, Y., Mita, N., Aoki, M. and Oppata, Y. (2015) Preliminary Report on Mineralogy and Geochemistry of Opals from the Shikaribetsu Area, Central Hokkaido. *Bulletin of the Geological Survey of Japan*, **66**, 169-178. https://doi.org/10.9795/bullgsj.66.169

[4] Kanai, Y., Tachibana, Y., Aoki, M., Okazaki, C., Oppata, Y., Mita, N., *et al.* (2016) Study on Chemical Composition of Fluorescent Opal Specimens in the Shikaribetsu Area, Central Hokkaido. *Bulletin of the Geological Survey of Japan*, **67**, 101-110. https://doi.org/10.9795/bullgsj.67.101

[5] Simoneit, B.R.T. and Fetzer, J.C. (1996) High Molecular Weight Polycyclic Aromatic Hydrocarbons in Hydrothermal Petroleums from the Gulf of California and Northeast Pacific Ocean. *Organic Geochemistry*, **24**, 1065-1077. https://doi.org/10.1016/s0146-6380(96)00081-2

[6] Emrarian, M., Sohrabi, M.R., Goudarzi, N. and Tadayon, F. (2021) Retention Time Prediction of Polycyclic Aromatic Hydrocarbons in Gas Chromatography-Mass Spectrometry Using QSPR Based on Random Forests and Artificial Neural Network. *Structural Chemistry*, **32**, 49-61. https://doi.org/10.1007/s11224-020-01614-9

[7] Ogihara, S. and Hirasawa, T. (2008) Analysis of C10-C13 Linear Alkylbenzenes by GC/MS. *Researches in Organic Geochemistry*, **23**/**24**, 131-138.

[8] Radke, M. (1988) Application of Aromatic Compounds as Maturity Indicators in Source Rocks and Crude Oils. *Marine and Petroleum Geology*, **5**, 224-236. https://doi.org/10.1016/0264-8172(88)90003-7

[9] Vaezzadeh, V., Yi, X., Rais, F.R., Bong, C.W., Thomes, M.W., Lee, C.W., *et al.* (2021) Distribution of Black Carbon and PAHs in Sediments of Peninsular Malaysia. *Marine Pollution Bulletin*, **172**, Article 112871. https://doi.org/10.1016/j.marpolbul.2021.112871

[10] Somerville, H.J., Bennett, D., Davenport, J.N., Holt, M.S., Lynes, A., Mahieu, A., *et al.* (1987) Environmental Effect of Produced Water from North Sea Oil Operations. *Marine Pollution Bulletin*, **18**, 549-558. https://doi.org/10.1016/0025-326x(87)90539-x

[11] Hylland, K. (2006) Polycyclic Aromatic Hydrocarbon (PAH) Ecotoxicology in Marine Ecosystems. *Journal of Toxicology and Environmental Health, Part A*, **69**, 109-123. https://doi.org/10.1080/15287390500259327

[12] Abdel-Shafy, H.I. and Mansour, M.S.M. (2016) A Review on Polycyclic Aromatic Hydrocarbons: Source, Environmental Impact, Effect on Human Health and Remediation. *Egyptian Journal of Petroleum*, **25**, 107-123. https://doi.org/10.1016/j.ejpe.2015.03.011

[13] Reizer, E., Viskolcz, B. and Fiser, B. (2022) Formation and Growth Mechanisms of Polycyclic Aromatic Hydrocarbons: A Mini-Review. *Chemosphere*, **291**, Article 132793. https://doi.org/10.1016/j.chemosphere.2021.132793

[14] Guerin, K., Murphy, D., Löhr, S.C. and Nothdurft, L. (2024) Experimental Constraints on the Role of Temperature and Pyrogenic Mineral Assemblage in Wildfire-Induced Major and Trace Element Mobilisation. *Geochimica et Cosmochimica Acta*, **386**, 18-32. https://doi.org/10.1016/j.gca.2024.10.015

[15] Certini, G. (2005) Effects of Fire on Properties of Forest Soils: A Review. *Oecologia*, **143**, 1-10. https://doi.org/10.1007/s00442-004-1788-8

[16] Simon, E., Choi, S. and Park, M. (2016) Understanding the Fate of Polycyclic Aromatic Hydrocarbons at a Forest Fire Site Using a Conceptual Model Based on Field Monitoring. *Journal of Hazardous Materials*, **317**, 632-639. https://doi.org/10.1016/j.jhazmat.2016.06.030

[17] Campos, I., Abrantes, N., Pereira, P., Micaelo, A.C., Vale, C. and Keizer, J.J. (2019) Forest Fires as Potential Triggers for Production and Mobilization of Polycyclic Aromatic Hydrocarbons to the Terrestrial Ecosystem. *Land Degradation & Development*, **30**, 2360-2370. https://doi.org/10.1002/ldr.3427

[18] Strunz, H. and Contag, B. (1965) Evenkite, Flagstaffite, Idrialite, and Refikite. *Neues Jahrbuch fur Mineralogie, Monatshefte*, **5**, 19-25.

[19] Murdoch, J. and Geissman, T.A. (1967) Pendletonite, a New Hydrocarbon Mineral from California. *American Mineralogist*, **52**, 611-616.

[20] Echigo, T., Kimata, M. and Shimizu, M., (2007) Crystalline Adamantane (C16H10) Co-Existed with Native Mercury from Itomuka Mine, Hokkaido, Japan. *Abstracts of the Frontiers in Mineral Sciences* 2007 *Conference*, Cambridge, 55.

[21] Dunning, G.E., Hadley, T.A., Magnasco, J., Christy, A.G. and Jr. Cooper, J.F. (2005) The Clear Creek. Mine, San Benito County, California: A Unique Mercury Locality. *Mineralogical Record*, **36**, 337-363.